Article

Diffusion Regulation in the Vitreous Humor

Benjamin Tillmann Käsdorf,[1,2] Fabienna Arends,[1,2] and Oliver Lieleg[1,2,*]
[1]Institute of Medical Engineering (IMETUM) and [2]Department of Mechanical Engineering, Technische Universität München, Garching, Germany

ABSTRACT   The efficient treatment of many ocular diseases depends on the rapid diffusive distribution of solutes such as drugs or drug delivery vehicles through the vitreous humor. However, this multicomponent hydrogel possesses selective permeability properties, which allow for the diffusion of certain molecules and particles, whereas others are immobilized. In this study, we perform an interspecies comparison showing that the selective permeability properties of the vitreous are conserved across several mammalian species. We identify the polyanionic glycosaminoglycans hyaluronic acid and heparan sulfate as two key macromolecules that establish this selective permeability. We show that electrostatic interactions between the polyanionic macromolecules and diffusing solutes can be weakened by charge screening or enzymatic glycosaminoglycan digestion. Furthermore, molecule penetration into the vitreous is also charge-dependent and only efficient as long as the net charge of the molecule does not exceed a certain threshold.

INTRODUCTION

Numerous ocular diseases, such as cataract, glaucoma, diabetic retinopathy, or age-related macular degeneration affect the quality of life of millions of people worldwide. Diseases concerning the anterior part of the eye, such as the lens, cornea, ciliary body, etc., allow an effective treatment via topical administration. However, therapy of diseases occurring in the posterior eye segment (except the choroid, which is densely perfused with blood vessels) is very challenging but necessary when the retina is concerned, as it is in cases of age-related macular degeneration, the third leading cause of blindness (1). Topical administration of drugs suffers from low efficiency due to poor drug penetration through barriers of the human eye such as the corneal epithelium, the tear film, or conjunctival absorption (2,3). Treatment of ocular diseases via systemic drug administration is mainly restricted by the blood-retinal barrier, which prevents free passage of xenobiotics from the choroid into the retina and the vitreous humor (4). Diffusion studies of various drugs have confirmed that penetration into the vitreous is much more restricted than into the aqueous humor (5). Macha et al. (6) studied the penetration of systemically applied fluorescein into the vitreous humor of rabbits and found that only 1–2% of the plasma levels of fluorescein can be detected in the vitreous. To achieve intraocular drug levels within the therapeutic range, the drug concentration in the blood stream would lead to severe systemic side effects (7,8).

Therefore, intravitreal injection is an attractive alternative delivery route of drugs to the posterior segment of the eye

that does not cause systemic side effects. Yet there are still major drawbacks related to intraocular injection, including patient noncompliance, the need for repeated injections, and injection-associated infections. In addition, the risks of complications increase with the frequency of injections (4). Another major issue is the residence time of drug molecules in the vitreous humor. For prolonged drug release, drug-loaded nanoparticles such as liposomes are used, which provide a long-lasting supply of intravitreal drug molecules while preventing them from degradation (9–12). When therapeutic drug molecules are deposited into the vitreous humor, whether alone or encapsulated in nanoparticles, a detailed knowledge about their intravitreal mobility is crucial for devising an optimal treatment strategy. However, depending on their size and surface properties, the diffusion of these objects can be strongly hindered in the vitreous (13,14).

The mammalian vitreous consists of a strongly hydrated extracellular matrix with a water content of >98%. The gel structure is mainly maintained by collagen fibrils (15). In addition to collagen II, glycosaminoglycans (GAGs) such as hyaluronic acid (HA), heparan sulfate (HS), and chondroitin sulfate are present in the vitreous gel (Fig. 1 a), yet in lower concentrations than collagen. The highly hydrated HA serves as a space-filling network between the collagen fibrils (16,17). Due to its heterogeneous distribution of macromolecules throughout the vitreous (18,19), as well as age-related changes in the molecular composition of the vitreous (20), the reported concentration of HA ranges from 65 to 400 $\mu g/mL$ for human and from 50 to 570 $\mu g/mL$ for bovine vitreous (19,21,22).

Xu et al. (13) estimated the mesh size of bovine vitreous to be ~550 nm and observed that 200 nm polystyrene
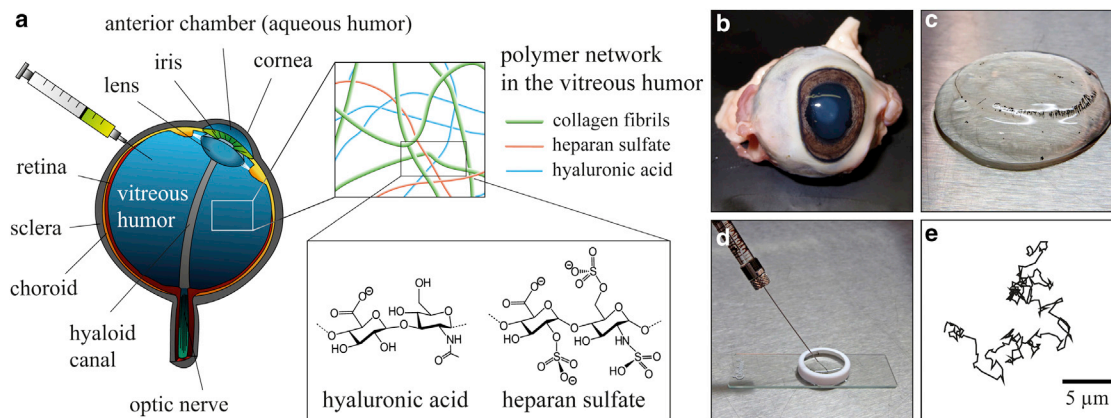
FIGURE 1 Schematic overview of a mammalian eye (*a*) and vitreous preparation process for SPT (*b–e*). (*a*) The vitreous humor of the mammalian eye mainly consists of collagen fibrils, as well as the GAGs HA and HS, both of which carry several negative charges. From fresh ovine eyes (*b*), the vitreous humor is carefully removed (*c*), and nanoparticles are injected into the vitreous (*d*). Trajectories characterizing the thermal motion of the nanoparticles in the vitreous humor (*e*) are obtained by optical microscopy. To see this figure in color, go online.

particles with negative COOH surface groups showed nearly free diffusion in the vitreous, whereas particles of the same size but with positive NH$_2$-functionalized surfaces were immobilized. A similar charge-dependent suppression of particle diffusion has also been observed in other biological hydrogel systems (23–27), which suggests that this might be a more generic filtering mechanism in biology (28). Hindered mobility for cationic particles in the vitreous, as well as improved mobility of particles coated with polyethylene glycol (PEG), has been reported by several other groups (13,14,29–31), indicating that the vitreous humor gel constitutes a selective diffusion barrier for particles. As a physical mechanism for this selective suppression of particle diffusion, a combination of electrostatic and hydrophobic interactions has been proposed (13,14,29,31). However, clear experimental evidence is still missing, and the detailed molecular components of the vitreous that establish those interactions still need to be identified.

One strategy to achieve this goal is comparing the diffusive mobility of well-defined model molecules or model nanoparticles in the vitreous. Polystyrene particles and liposomes are a well-suited particle platform for such an endeavor, since they can be obtained at comparable sizes but with different surface qualities. Especially tuning the net charge of liposomes is easily possible, e.g., by adjusting the lipid composition used for liposome generation. Similarly, when studying molecule diffusion in the vitreous, dextrans and oligopeptides offer the possibility of tuning two molecule properties, size and charge, independently. Dextrans are available at different molecular masses and can be obtained with different chemical modifications. Thus, they have a well-defined charge/molecular mass ratio, but this cannot easily be tuned. Synthetic oligopeptides, on the other hand, are a very versatile system, as one can create specific charge patterns or charge densities by linking up amino acids (almost) at will during synthesis. Therefore, with those test particles

and molecules, a broad range of solute sizes and solute net charges can be modeled, which allows for a systematic analysis of the permeability properties of the vitreous.

Here, we show that the selective permeability of the vitreous humor is largely based on electrostatic interactions between the biopolymer network and diffusing particles or molecules. This charge-selective suppression of diffusion seems to be a conserved mechanism across different mammalian species, as we observe identical behavior in the vitreous humor obtained from bovine, porcine, and ovine eyes. By enzymatic treatment of the vitreous, we identify the polyanionic GAGs HA and HS as two molecular key components that establish selective particle trapping. Removal of those macromolecules, as well as charge screening by high salt concentrations, entails mobilization of trapped particles. The charge-selective trapping ability of the vitreous also extends to molecules such as dextrans and peptides if their net charge is high enough.

MATERIALS AND METHODS

Test particles and molecules

Since the mesh size of bovine vitreous was estimated to be ~550 nm (13), a size of 200 nm for the particles and liposomes employed in this study was chosen to minimize steric hindrance effects.

Fluorescent polystyrene particles (carboxyl-terminated or amine-terminated) 200 nm in diameter were obtained from Invitrogen (Carlsbad, CA). Polyethylene glycol (PEG, molecular mass 750 Da, Rapp Polymere, Tübingen, Germany) coating of carboxyl-terminated beads was performed using a modified carbodiimide-coupling procedure based on the protocol described in Nance et al. (31). In brief, 100 μL of 200 nm carboxyl-terminated polystyrene particles was washed in ultrapure water and diluted fourfold to a final concentration of 0.5% solids. Next, 50 mM α-methoxy-ω-amino-PEG was added to the particle solution and mixed thoroughly, and 100 mM N-hydroxysulfosuccinimide sodium salt (sulfo-NHS, Sigma-Aldrich, St. Louis, MO) was mixed with the suspension. Then, 60 mM N-(3-dimethylaminopropyl)-N'-ethylcarbodiimide hydrochloride (EDAC, Sigma-Aldrich) was suspended in 600 μL borate buffer (pH 8.5) and mixed with the particle

suspension. Particles were incubated for 4 h at room temperature and then centrifuged and washed with ultrapure water.

Lipids were obtained from Avanti Polar Lipids (Alabaster, AL) in chloroform. Liposomes were prepared from 1,2-dioleoyl-*sn*-glycero-3-phosphocholine (DOPC), 1,2-dioleoyl-3-trimethylammonium-propane (DOTAP), 1,2-dioleoyl-*sn*-glycero-3-(phospho-rac-(1-glycerol)) (DOPG), and fluorescently labeled with 1,2-dioleoyl-*sn*-glycero-3-phosphoethanol-amine-N-(lissamine rhodamine B sulfonyl) (Rh-DOPE). Lipids were mixed to a total amount of 0.5 μmol with 5 mol % Rh-DOPE. For preparation of zwitterionic DOPC liposomes 90 mol % of DOPC and an additional 5 mol % DOTAP were mixed to compensate the negative charge of 5 mol % Rh-DOPE. For simplicity, those DOPC/DOTAP/Rh-DOPE liposomes are referred to as DOPC liposomes in this article. Solvent evaporation was conducted overnight to generate a thin lipid film. This lipid film was resuspended in 500 μL 10 mM phosphate buffer (pH 7.3, 154 mM NaCl) and mixed thoroughly. The suspension was then sonicated in an ultrasonic bath for 10 min to produce small unilamellar vesicles. These were extruded through a 0.2 μm polycarbonate membrane with a miniextruder (Avanti Polar Lipids) and stored at 4°C until further use.

Fluorescein-isothiocyanate labeled dextrans (4 kDa or 150 kDa) were obtained from Sigma-Aldrich. We used three dextran variants here: dextrans without modification (FITC-dextrans) and dextrans that have been modified with either carboxymethyl (FITC-CM-dextrans) or diethylaminoethyl groups (FITC-DEAE-dextrans). Stokes radii for the dextrans used here are 1.4 nm for the 4 kDa dextrans and 8.5 nm for the 150 kDa dextrans (according to the supplier's information).

Customized oligopeptides (total length, 24 amino acids, labeled at the N-terminus with 5-carboxytetramethylrhodamine (TAMRA)) were obtained from PEPperPRINT (Heidelberg, Germany). Anionic peptides had the sequences $(QQE)_8$ and $(EEE)_8$, and cationic peptides had the sequences $(QQK)_8$, $(QK)_{16}$, $(QKK)_8$, $(QKKKK)_4$, and $(KKK)_8$. Here, Q denotes glutamine (neutral at pH 7), E glutamic acid (negatively charged at pH 7), and K lysine (positively charged at pH 7). In the main text, those peptides are referred to as P1–P7, respectively, and details are given in Table S1 in the Supporting Material.

Size and ζ-potentials of polystyrene particles and liposomes were determined with dynamic light scattering using a Zetasizer Nano ZS (Malvern Instruments, Herrenberg, Germany) in 20 mM TRIS/HCl buffer (pH 7.3, 10 mM NaCl). To avoid osmotic pressure, lipids were resuspended in this buffer for size and ζ-potential measurements.

Furthermore, Table S1 gives an overview of the estimated number of net charges of particles and molecules used in this study.

Preparation of fresh vitreous samples

Due to the limited availability of fresh human vitreous humor from patients of similar age, samples from animal sources are much better suited for a systematic study where different experimental conditions are supposed to be probed. Here, fresh ovine, bovine, and porcine eyes (Fig. 1 *b*) were obtained from a local slaughterhouse and immediately placed on ice. Extraocular material was removed and the sclera was carefully incised without cutting into the vitreous humor. The intact vitreous humor (Fig. 1 *c*) was detached from the sclera and immediately used for further experiments.

Single-particle tracking

For single-particle tracking (SPT), either 200 nm fluorescent polystyrene particles or 200 nm liposomes were diluted in phosphate buffer (pH 7.3, 154 mM NaCl) to allow SPT. Of this solution, 2 μL was carefully injected (~0.3 μL/s) into the vitreous humor using a 10 μL Hamilton syringe (gauge 26s, point style 2), as depicted in Fig. 1 *d*. The samples were incubated for ~0.5 h on ice before particle-tracking measurements were initiated.

Fluorescence microscopy was conducted on an Axioskop 2 MAT mot microscope (Zeiss, Oberkochen, Germany) equipped with an LD Plan-Neofluar 40× objective (Zeiss). Images were acquired with a digital camera (Orca-R2 C10600, Hamamatsu, Shizuoka, Japan) at 16 fps using the software HCImageLive provided by Hamamatsu. Particle trajectories were obtained from those movies using the image analysis software OpenBox developed at the Technical University of Munich (32). To quantify the microscopic mobility of the test particles, the mean-squared displacement (MSD) was determined from the trajectory of motion of the particles as described before (23). In brief, the MSD can be determined from the trajectory, $\vec{r}(t)$, of a particle by $\mathrm{MSD}(\tau) = (1/N)\sum_{i=1}^{N}[\vec{r}(i\Delta t + \tau) - \vec{r}(i\Delta t)]^2$ and is related to the diffusion coefficient via $\mathrm{MSD}(\tau) = 2nD\tau$, where $n = 2$ is used for the quasi-two-dimensional trajectories, $\vec{r}(t) = (x(t), y(t))$ of the analyzed particles. With this procedure, apparent diffusion coefficients are obtained as we explicitly assume a linear dependence of the MSD on τ. Only the first 10% of the MSD(τ) data are used to determine this apparent diffusion coefficient to avoid artifacts arising from statistical limitations (33, 34). However, calculation of the MSD(τ) data includes the entire video length of 20 s.

Charge-screening experiments

For charge-screening experiments, fluorescent amine-terminated polystyrene particles (200 nm in diameter) were diluted in high-salt solution (1 M NaCl, 1 M KCl, 4 M NaCl, and 4 M KCl, pH 7). Of this solution, 10 μL was carefully injected (~0.3 μL/s) into ovine vitreous humor using a 10 μL Hamilton syringe (gauge 26s, point style 2). A higher injection volume compared to the previous SPT experiments was used to achieve a high local concentration of ions in the vitreous. The samples were incubated for 5–15 min on ice before particle-tracking measurements were initiated. The time window between injection and SPT was shortened to ensure that the first measurement was conducted before the concentration of injected ions could equilibrate throughout the vitreous. For each sample, a second measurement was conducted at the same site in the vitreous humor 2 h after the first measurement. We verified that this shortened waiting time, as well as the increased injection volume, did not affect the mobility of the injected particles compared to the experimental conditions chosen for the rest of the SPT experiments (see Fig. S3). Furthermore, additional control experiments confirmed that injecting high-salt solutions into the vitreous did not disrupt the mechanical integrity of the vitreous (see Figs. S4 and S5).

Enzymatic digestion of ovine vitreous humor

For enzymatic digestion, the wet weights of ovine vitreous were determined, and afterward, the whole vitreous was submerged in an equal volume of digestion buffer. For HA digestion, 100 units of hyaluronidase from *Streptomyces hyalurolyticus* (H1136, Sigma-Aldrich) was dissolved in 100 mM sodium acetate buffer (pH 5.7, 77 mM NaCl, 0.01% BSA) for each vitreous humor. For HS digestion, 10 units of a blend of heparinase I and III from *Flavobacterium heparinum* (H3917, Sigma-Aldrich, St. Louis, MO, USA) were dissolved in 20 mM Tris/HCl buffer (pH 7.5, 50 mM NaCl, 0.01% BSA, 4 mM CaCl₂) for each vitreous humor. The following protease inhibitors were added to each buffer: 2 mM phenylmethanesulfonylfluoride (Carl Roth, Karlsruhe, Germany) and 5 mM benzamidine hydrochloride (Carl Roth). All enzymatic digestions were performed at 37°C for 72 h in 50 mL centrifuge tubes. Control samples were incubated in the same buffers but without enzymes. After digestion, wet weights of the vitreous samples were determined again to analyze the loss in water content due to enzymatic treatment. Afterward, vitreous samples were washed in phosphate buffer (pH 7.3, 154 mM NaCl) to get rid of residual HA/HS fragments. Particle-tracking measurements were performed in the vitreous to determine the apparent diffusion coefficients, as described above.

To verify the successful removal of HA and HS from fresh vitreous samples, HA and HS concentrations were determined by competitive enzyme-linked immunosorbent assay (ELISA) using commercial kits (Sheep HA

Elisa Kit and Sheep HS Elisa Kit, BlueGene, Shanghai, China). Therefore, treated and untreated vitreous samples were homogenized with a pipette and centrifuged at 1000 rcf for 15 min. Then, the supernatant was used for quantifying the concentrations of HA and HS with the ELISA kits using purifed HA and HS samples as calibration standards.

FITC-dextran and peptide penetration into the vitreous humor

Whole ovine vitreous humor samples or vitreous fragments were placed into FITC-dextran solutions in a 50 mL centrifuge tube so that the samples were fully submerged. Per gram of vitreous sample, 0.2 mL of dextran solution was used. Dextrans were dissolved at a concentration of 10 mg/mL in 10 mM phosphate buffer (pH 7.3, 154 mM NaCl). After incubation at 4°C overnight in the dark, the samples were washed in 10 mM phosphate buffer (pH 7.3, 154 mM NaCl) to remove remaining FITC-dextrans from the surface. The samples were homogenized with a pipette, and three samples of 100 μL each were taken for quantification. Fluorescence intensities were measured with a plate reader (VICTOR X3 Multilabel Plate Reader, Perkin-Elmer, Waltham, MA) at an excitation wavelength of 485 nm and emission wavelength of 535 nm. The same procedure was used for studying oligopeptide penetration into the vitreous humor. There, the peptide concentration was 1 mg/mL and again 0.2 mL of this solution was used per gram of vitreous sample tested. The wavelengths used for fluorescence measurements with peptides were 570 nm for excitation and 642 nm for emission.

Statistical analysis

To determine whether the differences between the examined groups are significant, one-way analyses of variance (ANOVAs) and Tukey post hoc tests were carried out. The Shapiro-Wilk test of normality and the Levene's test for homogeneity of variances were used to verify the assumptions of normal distribution and homogeneity of variances. Differences were considered to be statistically significant for $p < 0.01$. All statistical analyses were performed using R (Foundation for Statistical Computing, Vienna, Austria).

RESULTS AND DISCUSSION

Vitreous humor selectively traps charged polystyrene particles

Similar to previous studies on vitreous permeability (13,14,29), bovine vitreous was chosen for the initial experiments. First, we compare the diffusion coefficients of different polystyrene particles, i.e., amine- and carboxyl-

terminated particles, as well as PEGylated particles, all with a diameter of 200 nm in fresh bovine vitreous humor. As illustrated in Fig. 2 a, the MSD curves calculated from the trajectories of amine-terminated particles can be divided into two groups: a small fraction of the MSD curves depend linearly on τ, which indicates free diffusion. However, the larger fraction exhibits subdiffusive behavior, with MSD curves that only weakly increase with τ, demonstrating that the motion of the corresponding particles is strongly hindered. Apparent diffusion coefficients (D_{app}) calculated from those MSD curves (Fig. 2 b) underscore this impression: the small, mobile fraction of the particles exhibit an apparent diffusion coefficient, which amounts to 25% of the theoretical value of free diffusion in water (D_{free}). In contrast, for the larger fraction of particles with subdiffusive MSD curves, we obtain apparent diffusion coefficients with $D_{app} < 10\%$ of D_{free}, which indicates that the vitreous humor hydrogel constitutes a significant diffusion barrier for these amine-terminated particles. At the same experimental conditions, carboxyl-terminated particles can also be subdivided into nearly freely diffusing and strongly subdiffusive particles (Fig. 2 b); however, the subdiffusive part of the population is significantly smaller than for the amine-terminated particles. In contrast, PEGylated particles show a nearly Gaussian distribution of apparent diffusion coefficients centered at a value of 50% of D_{free} (Fig. 2 b), and the immobile fraction is missing for this particle variant. These findings confirm previous results showing that the diffusive mobility of polystyrene particles in bovine vitreous humor strongly depends on the surface properties of the particles, and that the charge of the particle surface is a key parameter as cationic surface groups reduce the particle mobility.

Such a bimodal distribution of D_{app} has already been observed for polystyrene particles and polyplexes in bovine vitreous (14) which demonstrates that our results can be directly compared to previous studies on vitreous permeability. There, however, ensemble-averaged diffusion coefficients were calculated from those bimodal distributions, which is different from our categorization approach into
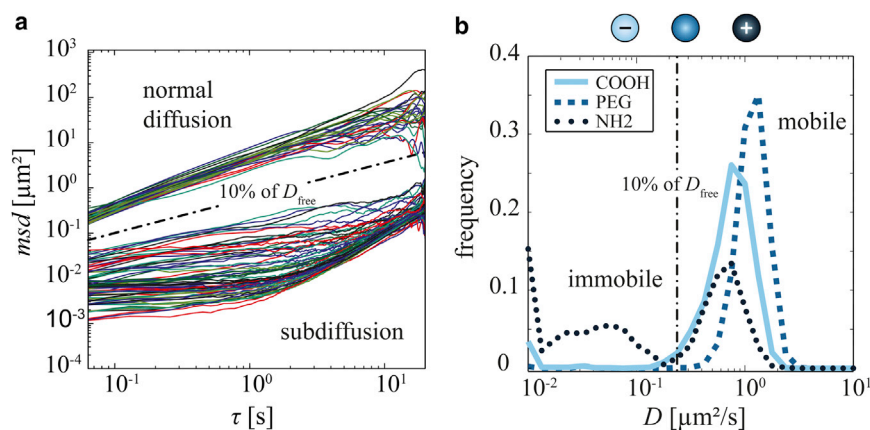

FIGURE 2 Diffusive mobility of 200 nm polystyrene particles in bovine vitreous humor. (a) MSD curves calculated from the individual trajectories of amine-terminated 200 nm polystyrene particles in bovine vitreous humor. (b) The distribution curves contain data from >1000 apparent diffusion coefficients from carboxyl-terminated (COOH), PEGylated (PEG), and amine-terminated (NH$_2$) 200 nm polystyrene particles in bovine vitreous humor. The dash-dotted line in both graphs is located at 10% of the diffusion coefficient of 200 nm particles in water (D_{free}). Using this line as a threshold, the particle ensemble can be divided into a mobile and an immobile fraction. To see this figure in color, go online.
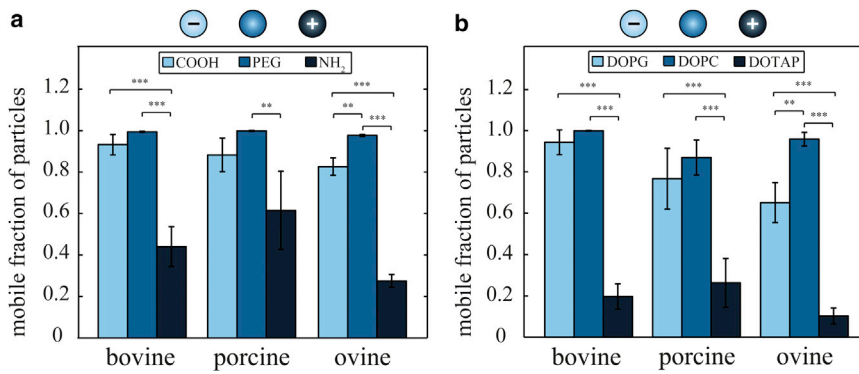
FIGURE 3 Interspecies comparison of the diffusive mobility of polystyrene and liposome particles in vitreous. (*a*) Comparison of the mobile fraction ($D_{app} > 10\%$ of D_{free}) of carboxyl-terminated (COOH), PEGylated (PEG), and amine-terminated (NH$_2$) 200 nm polystyrene particles in bovine, porcine, and ovine vitreous humor. (*b*) Comparison of the mobile fractions ($D_{app} > 10\%$ of D_{free}) of DOPG, DOPC, and DOTAP 200 nm liposomes in bovine, porcine, and ovine vitreous humor. Several hundred particle trajectories were acquired per sample and then categorized into mobile and immobile fractions. The error bars denote the standard deviation for those fractions as obtained from at least three vitreous samples. Asterisks denote statistically significant differences (**$p < 0.01$; ***$p < 0.001$). To see this figure in color, go online.

mobile and immobile particle fractions. Here, the bimodal distribution was most pronounced for amine-terminated particles. This could arise from transient particle trapping and escape events, as previously observed in basal lamina hydrogels (35). In the vitreous, weak or strong particle trapping could, e.g., originate from an inhomogeneous distribution of biopolymers (18,19). Areas with a higher density of macromolecules could result in more tightly trapped particles than areas with fewer macromolecules.

Interspecies comparison of the mobility of polystyrene particles and liposomes

Previous in vitro experiments on vitreous permeability have mostly been conducted using bovine vitreous (13,14). To test whether the observed charge-dependent nanoparticle mobility is conserved across species, we next compare the diffusive mobility of polystyrene particles in bovine, porcine, and ovine vitreous humor. In all vitreous variants, we observe a bimodal distribution of apparent diffusion coefficients for charged polystyrene particles, similar to what we discussed for bovine vitreous (see Fig. S1). Thus, in all cases, we can subdivide the analyzed particle ensembles into an immobile ($<10\%$ of D_{free}) and a mobile ($>10\%$ of D_{free}) fraction. Fig. 3 *a* displays this fraction of mobile particles in an interspecies comparison. This comparison returns a similar picture for porcine, bovine, and ovine vitreous humor: almost 100% of the PEGylated particles, as well as 80% of the carboxyl-terminated particles, are mobile in all vitreous samples. However, the trapping of amine-terminated particles seems to be somewhat stronger in ovine vitreous than in the other two vitreous variants, as we find only 25% mobile particles here compared to ~45–50% in porcine and bovine vitreous.

Having confirmed that the diffusive mobility of polystyrene particles in the vitreous humor of various species depends on the surface properties of the particles, we next ask whether the chemical origin of the particle charge is relevant for the suppression of particle diffusion. In other words, we aim to test whether unspecific electrostatic interactions or specific binding between the amino groups of polystyrene particles and vitreous components are responsible for particle trapping. To tackle this question, we next investigate the diffusive mobility of a second particle system in addition to polystyrene particles. Liposomes constitute a suitable platform for this purpose for two reasons: on the one hand, the overall net charge of liposomes can be easily tuned by mixing lipids with different headgroups, and the size of the liposomes can be controlled by extrusion. On the other hand, liposomes are medically highly relevant particles, as they are widely used as a carrier system for therapeutic drug delivery.

To allow for a direct comparison to the data obtained with polystyrene particles, we chose 200 nm as an average size for the liposome particles (see Materials and Methods). As shown in Fig. 3 *b*, the diffusive mobility of such 200 nm liposomes in vitreous humor is very similar to that of polystyrene particles of similar ζ-potential (see Table 1). The majority of zwitterionic (DOPC) and anionic (DOPG) liposomes remain mobile in the vitreous, whereas the diffusion of cationic (DOTAP) liposomes is largely suppressed. Again, a bimodal distribution of apparent diffusion coefficients for these cationic liposomes is observed (see Fig. S2), and these results are obtained in all three vitreous variants. These findings demonstrate that indeed a positive particle surface charge is responsible for the reduction in particle mobility and that no specific chemical motif is

TABLE 1 **Particle characterization**

	Particle Type	Particle Size (nm)	PDI	ζ pH 7,3 (mV)
Polystyrene particles	carboxyl	222	0.033	-34.7 ± 1.0
	PEG	231	0.024	-11.4 ± 1.6
	amine	253	0.087	$+7.5 \pm 1.7$
Liposomes	DOPG	185	0.24	-50.2 ± 1.7
	DOPC	194	0.26	$+1.3 \pm 0.3$
	DOTAP	171	0.19	$+41.0 \pm 0.8$

Particle size, polydispersity index (PDI), and particle ζ-potential are determined from dynamic light scattering for polystyrene particles and liposomes.

required to induce particle immobilization. Of course, liposomes differ from polystyrene beads in terms of surface charge mobility and mechanical deformability. Yet, as we observe identical charge-dependent immobilization behavior of those two particle species in vitreous, these differences in the particle properties seem not to be crucial for what we describe here.

Our finding that the selective permeability properties of the vitreous seem to be conserved across several mammalian species suggests that the results gained here can, to a certain degree, be extrapolated to other mammalian vitreous variants, including human vitreous. For all vitreous variants tested here, we detect a weak trapping of negatively charged particles, which is most prominent for ovine vitreous samples. This finding is in agreement with previous studies on nanoparticle diffusion in bovine vitreous, where it was suggested to arise from hydrophobic interactions between the polystyrene particles and collagen II fibers (13,14,29). However, we observe a similar low fraction of trapped negatively charged DOPG liposomes, and those liposomes should not be able to engage in hydrophobic interactions. In any case, the trapping efficiency of negatively charged particles is clearly less dominant compared to the trapping of positively charged particles.

For the remainder of the article, we aim at identifying the molecular mechanism and the vitreous components that give rise to this trapping of positively charged particles. We approach this goal by employing different strategies to re-mobilize trapped particles and drawing conclusions from the change in experimental conditions that are required for such a remobilization. As we found ovine vitreous to possess the strongest trapping efficiency for amine-terminated particles, all following experiments were conducted with ovine vitreous. Furthermore, since high-salt injections

into the vitreous gel might compromise the stability of liposomes (due to osmotic pressure effects), polystyrene particles were used for the remobilization experiments.

High salt concentrations prevent particle immobilization

If electrostatic interactions between the polymer network of the vitreous humor and particles are mainly responsible for the observed suppression of particle diffusion, these interactions (and therefore the microscopic mobility of charged particles) should depend on the ion content of the vitreous. At higher ionic strength of the vitreous, exposed surface charges of particles or vitreous biopolymers will be partially shielded by a layer of counterions (Fig. 4 a), resulting in a reduction of the electrostatic interaction potential. The strength of this charge screening will increase with rising ion concentrations. Therefore, in a next set of experiments, we injected amine-terminated polystyrene particles together with a high-salt buffer to locally increase the ion concentration in ovine vitreous humor and then determine the mobility of the particles.

Fig. 4 b shows the results of such a charge screening experiment. When 10 μL of 1 M KCl are injected together with the amine-terminated particles into ovine vitreous humor, the mobile fraction of particles is increased from ~25% (physiological salt conditions of 154 mM) to ~45%. Consistently, a stronger increase of the local salt concentration, as achieved by injecting 10 μL of 4 M KCl, results in an even higher mobile particle fraction of ~70%. This effect has been observed before in another hydrogel system (35) and confirms our notion that the mobility of trapped particles in the vitreous can be restored by inducing electrostatic screening, and that the strength of this effect can be
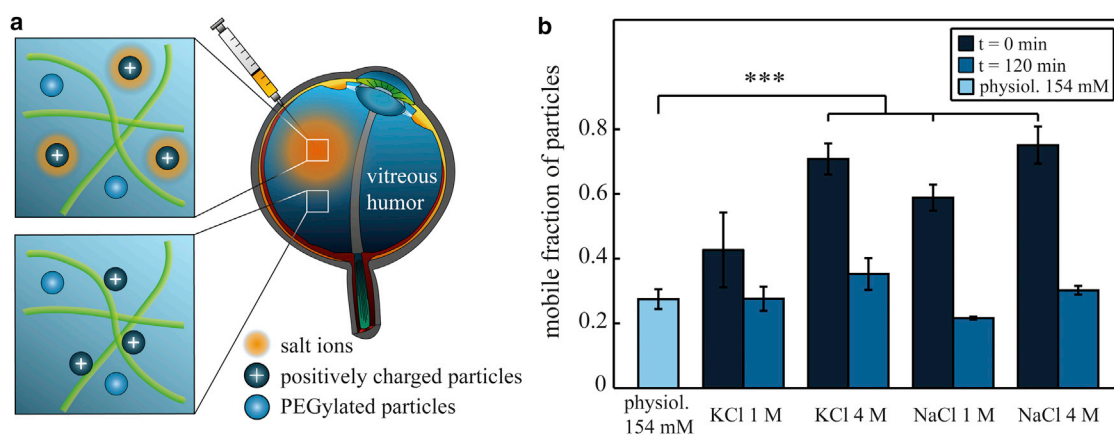

FIGURE 4 The mobility of trapped particles can be restored via charge screening. (a) Schematic illustration of charge screening as induced by ions (orange cloud) that are added to the vitreous. Charged particles (or polymers of the vitreous) concentrate counterions around their surface and thus avoid electrostatic trapping. (b) When KCl or NaCl is injected together with the particles, the mobile fraction of amine-terminated (NH$_2$) 200 nm polystyrene particles in ovine vitreous humor is increased compared to physiological salt concentrations (154 mM). At 2 h after injection, this remobilization effect is not present any more. More than 1000 particle trajectories were analyzed per experimental condition and categorized into mobile and immobile particle fractions. The error bars denote the standard deviation for those fractions as obtained from at least three vitreous samples. Asterisks denote statistically significant differences compared to physiological salt conditions (***$p < 0.001$). To see this figure in color, go online.

modulated by the amount of ions added to the vitreous. However, according to the Debye-Hückel theory (36), the strength of this screening process should only depend on the valency and concentration of the added ions, and not on the particular ion species. To test this prediction, we repeat the screening experiments with NaCl solutions. Indeed, we find that the injection of 10 μL of either 1 M or 4 M NaCl results in an increase of the mobile particle fraction similar to that observed for KCl injection, which suggests that this remobilization effect is not ion specific.

Since the increase in ion concentration in the vitreous gel is only induced locally, diffusive spreading of the injected ions through the vitreous should lead to a drop in the local ion concentration over time. We estimate the volume of each ovine vitreous sample by weighing and approximating the density of the gel by that of water. With the low injection volume of 10 μL used here, we then can calculate that the salt concentration in the vitreous should equilibrate at ~160 mM after a few hours. Consequently, the charge shielding effect will probably not be measurable any more when the salt concentration has equilibrated. Indeed, such a behavior is observed when the mobility of amine-terminated particles is determined again 2 h after injection (Fig. 4 b). For all salt-injection experiments, the fraction of mobile amine-terminated particles returns to ~20–30%, which matches the amount of mobile particles at physiological ion concentrations. These data underline our previous notion that particles can be trapped in the vitreous via electrostatic forces, and that this electrostatic trapping can be countered by charge screening.

However, full mobilization of the particle ensemble could not be achieved at our experimental conditions. A second physical mechanism that could counteract particle mobilization at high salt concentrations could be a gain in entropy due to the replacement of a layer of condensed counterions by charged macromolecules or polystyrene particles. This could occur as a consequence of particle binding to the hydrogel macromolecules and thus might support particle trapping. However, for HA, the Manning criteria for counterion condensation (37) are not fulfilled: the ratio of Bjerrum length and line charge of HA gives a value of 0.7, which corresponds to full ionization. HS carries three to four times the line charge of HA, so the ratio of Bjerrum length and line charge results in a value of 2.1–2.8. Thus, Manning's criterion seems to be fulfilled for HS. However, counterion condensation is dominant only as long as the Debye length is larger than the distance between two charges on the macromolecule (38). At physiological conditions as they apply to our vitreous samples, the Debye length is <1 nm, which corresponds to the distance between two charges on HA. At ion concentrations as high as 1 M (4 M), the Debye length is only ~0.3 nm (0.15 nm), which is even lower than the distance between two charged groups on HS. Finally, we observe that the mobilization of particles depends on the salt concentration. Yet, if Manning condensation were to play a crucial role for immobilizing particles in the vitreous humor, the fraction of trapped particles should be independent of the ion concentration.

As mentioned before, even with injection of 4 M NaCl or KCl, full particle mobilization could not be achieved. We speculate that the residual fraction of trapped particles at high ionic strength could be related to the trapping of negatively charged particles at physiological salt and arise from hydrophobic interactions between the polystyrene particles and vitreous components. As an alternative, even during the short waiting time between salt injection and measurement initiation, the injected ions could have partially been equilibrated—at least at the edge of the injection bolus—thus leading to incomplete particle mobilization.

Enzymatic digestion of polyanionic GAGs increases the fraction of mobile particles

Having shown that electrostatic forces are responsible for the immobilization of positively charged particles, we now set out to identify the key components of the vitreous humor that are involved in this trapping process. The vitreous humor comprises different polymers such as collagen type II and several GAGs, some of which carry polyanionic charges. Several carboxyl, as well as sulfate, groups introduce multiple negative charges into the network (Fig. 1 a). As shown in Fig. 4, electrostatic interactions between particles with positive surface charges and the vitreous humor network are responsible for a reduction of particle mobility. To identify the involved polymers we performed a separate enzymatic removal of the negatively charged HA and HS from ovine vitreous humor (Fig. 5). Digestion of collagen II from bovine and chick vitreous results in a loss of structural integrity of the vitreous gel (39,40), and we observe the same behavior for ovine vitreous (see Fig. S6). In contrast, the digestion of HS and HA leads to a decrease in the wet weight of the vitreous (see Table S2) but with its structural integrity maintained (see Figs. S7 and S8).

Enzymatic degradation of HA results in an increase of the mobile fraction of positively charged polystyrene particles to ~45% compared to ~25% in fresh, untreated vitreous and 15% in control samples that were stored in digestion buffer but in the absence of enzymes (Fig. 5). This result clearly indicates that this GAG is involved in the trapping of positively charged particles. Similarly, when the polyanionic GAG HS is digested, the mobile particle fraction is increased to ~40%. In the control groups, we observe a slight decrease of the mobile polystyrene particle fraction compared to fresh, untreated samples. We speculate that this reduction in particle movement could be due to loss of water of the vitreous gels over time, which even occurs to a certain degree when no vitreous components are removed by enzymatic treatment (see Table S2). Such a partial loss of water would entail a decreased gel mesh size and thus a reduced diffusive mobility of the polystyrene particles compared to fresh vitreous.
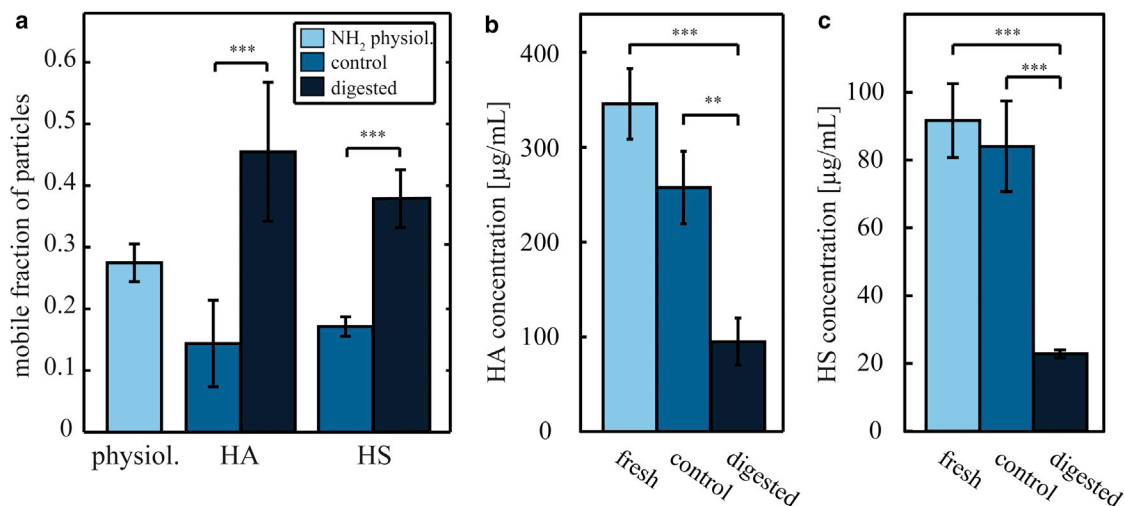
FIGURE 5 Enzymatic degradation of the polyanionic GAGs HA and HS in ovine vitreous increases particle mobility. (*a*) The mobile fraction ($D_{app} > 10\%$ of D_{free}) of amine-terminated (NH_2) 200 nm polystyrene particles after 72 h GAG digestion in ovine vitreous humor is compared to the mobile fraction of those particles in undigested vitreous. The control samples have been incubated in digestion buffer without enzymes. More than 1000 particle trajectories were analyzed per experimental condition and categorized into mobile and immobile particle fractions. The error bars denote the standard deviation for those fractions as obtained from at least three vitreous samples. (*b* and *c*) The concentration of HA and HS in fresh, untreated vitreous, as well as digested samples and control samples, was determined via competitive ELISA. Please note the different *y*-axis scaling for HA and HS. Asterisks denote statistically significant differences (**$p < 0.01$; ***$p < 0.001$). To see this figure in color, go online.

Therefore, statistical differences were only determined between digested and control vitreous samples, and we did not compare data from treated samples to physiological conditions. Fig. 5, *b* and *c*, depicts the measured concentrations of HA (Fig. 5 *b*) and HS (Fig. 5 *c*) in fresh, untreated vitreous compared to digested and control samples. The HA concentration in fresh ovine vitreous is ~350 μg/mL and thus in a range similar what has been measured in human and bovine vitreous (19,21,22). After enzymatic treatment of ovine vitreous, a strong decrease of HA and HS concentrations is observed, which suggests a direct link between HA/HS concentration in the vitreous and the diffusive mobility of amine-terminated polystyrene particles. HA and HS differ in terms of both their charge density and their concentration in the vitreous: HS carries three to four times as many negatively charged groups per length unit as HA, but HA is present at approximately fourfold the concentration of HS in ovine vitreous. In conclusion, both enzymatic treatments should have removed a similar amount of charged groups from the vitreous, and we find that both treatment strategies entail a similar outcome in terms of particle mobilization. This result may indicate that the total (local) amount of charge rather than the local charge density may be the relevant parameter that sets the trapping efficiency of solutes in the vitreous biopolymer network.

The vitreous can selectively prevent penetration of molecules

So far, we have analyzed the selective trapping mechanism of the vitreous using test particles as permeability probes.

Particle mobility in the vitreous is medically relevant, as injection of nanoparticles is used for the treatment of certain eye diseases (12,41–47). However, a much more regular treatment strategy employs the delivery of antibiotics through the vitreous to the posterior part of the eye. Such antibiotics are considerably smaller than the nanoparticles studied so far. Thus, in a last step, we test whether the selective permeability properties of the vitreous are also efficient on a molecular scale. As test molecules, we choose dextrans. They are available with various chemical modifications and, at the same time, with different well-defined molecular masses. In detail, we compare fluorescently labeled 4 kDa and 150 kDa dextrans with DEAE or CM groups to unmodified dextrans. Thus, we can explore the difference in diffusion behavior between positively charged, negatively charged, and neutral molecules.

However, SPT is not feasible with those molecules. Accordingly, we switch to macroscopic penetration tests for these experiments (see Materials and Methods). Fig. 6 *a* gives an overview of the penetration efficiency of different FITC-dextran molecules in ovine vitreous humor. Similar to the diffusion of nanoparticles studied before, we observe a different behavior for the 150 kDa dextran variants as a function of their charge: whereas unmodified (i.e., neutral), as well as polyanionic, CM-dextrans efficiently penetrate the vitreous and reach similarly high concentrations on the order of 1 mg/mL, the polycationic DEAE-dextrans show a much lower penetration efficiency and accumulate at the surface of the vitreous (Fig. S10). This demonstrates that the charge-selective permeability of the vitreous is similarly efficient on a molecular scale, at least
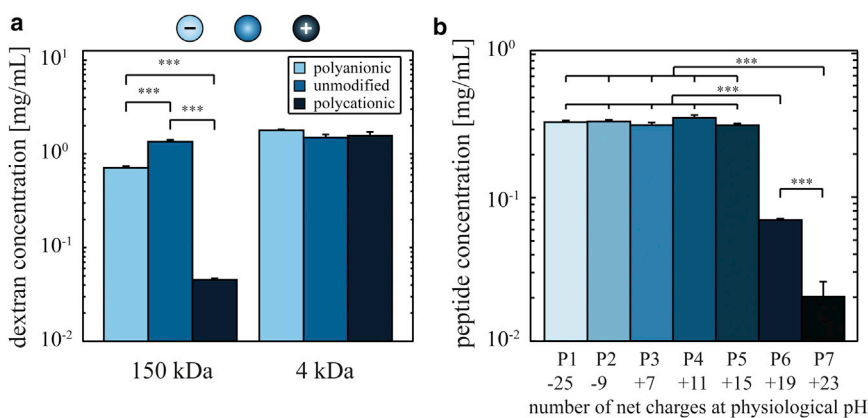
FIGURE 6 Penetration efficiency of different dextran molecules and oligopeptides into ovine vitreous humor. The concentrations of dextrans (*a*) and peptides (*b*) in ovine vitreous humor are shown after incubation of the vitreous samples overnight in different dextran/peptide solutions. DEAE (polycationic), unmodified (neutral), and CM (polyanionic) dextrans are compared at two different molecular masses (*a*). The sequence of the peptides P1–P7 (*b*) is described in Materials and Methods and in the Supporting Material. The error bars denote the standard deviation as obtained from three vitreous samples. Asterisks denote statistically significant differences (***$p < 0.001$). To see this figure in color, go online.

for those 150 kDa dextran molecules. However, when smaller dextrans (4 kDa) are used in those penetration experiments, we do not detect any significant differences between the three dextran variants (Fig. 6 *a*).

Very similar results are obtained when the vitreous samples are divided into three to four fragments before the penetration experiments are conducted (Fig. S11), which demonstrates that our penetration tests indeed probe the bulk permeability of the vitreous. It is important to realize that the 4 kDa dextran molecules carry only about three to five positive charges per molecule, which is very low compared to the number carried by larger 150 kDa variants, i.e., 160–200 charges per molecule. Considering that both dextran variants are significantly smaller than the mesh size of the vitreous and have similar charge densities (i.e., a similar net charge per molecular mass), this indicates the existence of a charge threshold above which the diffusion of solutes is suppressed by the vitreous.

To better characterize this charge threshold, we switch to another molecule model system, which allows for better tuning the molecular net charge at a fixed molecular mass. Synthetic oligopeptides can be generated with specific charge patterns, and therefore, varying the net charge on those molecules is easily possible. We here compare anionic peptides (carrying either −25 or −9 charges) to several cationic peptides (carrying either +7, +11, +15, +19, or +23 charges). Fig. 6 *b* depicts the penetration efficiency of these different oligopeptide species into ovine vitreous. All peptides possess a molecular mass of ~4 kDa. The anionic peptides, as well as some cationic species (P1–P5), efficiently penetrate the vitreous (Fig. S12 a). However, the strongly cationic species with 19 positive charges (P6) exhibits a strongly reduced penetration efficiency into the vitreous, and the polylysine oligopeptide (P7, +23 charges) is virtually unable to penetrate the vitreous but accumulates on the surface (Fig. S12 b). These findings are in good agreement with the results from the dextran penetration experiments and support the idea that a charge threshold exists above which the diffusion of molecules in the vitreous polymer

network is strongly suppressed. Whereas polycationic peptides with up to 15 positive charges per molecule are able to penetrate the vitreous with a high efficiency, the vitreous constitutes an efficient barrier for highly cationic peptides. This results either in a strongly reduced penetration efficiency of such molecules (P6, +19 charges) or even an almost complete blocking of penetration (P7, +23 charges).

Whereas nanoparticles (13,14) may easily exceed this charge threshold, antibiotics are typically only weakly charged, similar to the 4 kDa dextrans and peptides studied here. This suggests that if nanoparticles with suitable surface charges are used as drug carriers for intravitreal injection, diffusive spreading of antibiotics through the vitreous will probably not be strongly hindered. This offers the possibility to combine drug-delivery carriers (such as nanoparticles) and drug molecules with different immobilization efficiencies in the vitreous to tailor the distribution/retention times of nanoparticles and the enclosed drugs independently. One could imagine a scenario where injected drug-loaded nanoparticles are supposed to remain strongly localized, e.g., when they are deposited close to the retina to treat a retinal disease. This would then guarantee an efficient delivery of the embedded drugs to the target site and still allow for tuning the drug mobility/retention in the vitreous. The latter can be affected by various factors, e.g., the structure or charge state of the drug molecules. Typical half-life values of antibiotics are usually in the range of only several hours (48). Conversely, for a more global treatment of ocular diseases, nanoparticles with a high mobility in the vitreous could be advantageous. Particles with neutral or negative net charges should be equally suitable for this second scenario.

CONCLUSION

Here, we have shown that the ability of the vitreous humor to suppress diffusion of solutes is largely based on electrostatic interactions, which are mediated by the polyanionic GAGs HA and HS. Together with previous results from other

studies, our findings indicate that the biopolymers comprising the vitreous fulfill very different tasks: collagen II is mainly responsible for providing the vitreous with its mechanical properties and maintaining the structural integrity of the hydrogel. In contrast, the GAGs bind water and regulate the diffusion of particles and molecules within the hydrogel. Such a complementary function of biomacromolecules is also observed in other collagen/GAG hybrid systems such as the basal lamina and articular cartilage. This highlights the generic role polyanionic GAGs assume in setting up the complex material properties of tissues.

SUPPORTING MATERIAL

Supporting Materials and Methods, twelve figures and two tables are available at http://www.biophysj.org/biophysj/supplemental/S0006-3495(15)00112-4.

AUTHOR CONTRIBUTIONS

B.T.K., F.A., and O.L. proposed the experiments. The experiments were performed by B.T.K. Data analysis was performed by B.T.K. and F.A. The article was written by B.T.K., F.A., and O.L.

ACKNOWLEDGMENTS

REFERENCES

1. Resnikoff, S., D. Pascolini, …, S. P. Mariotti. 2004. Global data on visual impairment in the year 2002. *Bull. World Health Organ.* 82:844–851.

2. Bochot, A., B. Mashhour, …, E. Fattal. 1998. Comparison of the ocular distribution of a model oligonucleotide after topical instillation in rabbits of conventional and new dosage forms. *J. Drug Target.* 6:309–313.

3. Hughes, P. M., O. Olejnik, …, C. G. Wilson. 2005. Topical and systemic drug delivery to the posterior segments. *Adv. Drug Deliv. Rev.* 57:2010–2032.

4. Duvvuri, S., S. Majumdar, and A. K. Mitra. 2003. Drug delivery to the retina: challenges and opportunities. *Expert Opin. Biol. Ther.* 3:45–56.

5. Cunha-Vaz, J. G. 1976. The blood-retinal barriers. *Doc. Ophthalmol.* 41:287–327.

6. Macha, S., and A. K. Mitra. 2001. Ocular pharmacokinetics in rabbits using a novel dual probe microdialysis technique. *Exp. Eye Res.* 72:289–299.

7. Henderly, D. E., W. R. Freeman, …, N. A. Rao. 1987. Cytomegalovirus retinitis and response to therapy with ganciclovir. *Ophthalmology.* 94:425–434.

8. Jabs, D. A., C. Newman, …, B. F. Polk. 1987. Treatment of cytomegalovirus retinitis with ganciclovir. *Ophthalmology.* 94:824–830.

9. Meisner, D., J. Pringle, and M. Mezei. 1989. Liposomal ophthalmic drug delivery. III. Pharmacodynamic and biodisposition studies of atropine. *Int. J. Pharm.* 55:105–113.

10. Kurz, D., and T. A. Ciulla. 2002. Novel approaches for retinal drug delivery. *Ophthalmol. Clin. North Am.* 15:405–410.

11. Bochot, A., P. Couvreur, and E. Fattal. 2000. Intravitreal administration of antisense oligonucleotides: potential of liposomal delivery. *Prog. Retin. Eye Res.* 19:131–147.

12. Kaur, I. P., A. Garg, …, D. Aggarwal. 2004. Vesicular systems in ocular drug delivery: an overview. *Int. J. Pharm.* 269:1–14.

13. Xu, Q., N. J. Boylan, …, J. Hanes. 2013. Nanoparticle diffusion in, and microrheology of, the bovine vitreous ex vivo. *J. Control Release.* 167:76–84.

14. Martens, T. F., D. Vercauteren, …, K. Braeckmans. 2013. Measuring the intravitreal mobility of nanomedicines with single-particle tracking microscopy. *Nanomedicine (Lond.).* 8:1955–1968.

15. Bishop, P. 1996. The biochemical structure of mammalian vitreous. *Eye (Lond.).* 10:664–670.

16. Scott, J. E. 1992. The chemical morphology of the vitreous. *Eye (Lond.).* 6:553–555.

17. Bishop, P. N. 2000. Structural macromolecules and supramolecular organisation of the vitreous gel. *Prog. Retin. Eye Res.* 19:323–344.

18. Balazs, E. A., T. C. Laurent, and U. B. Laurent. 1959. Studies on the structure of the vitreous body. VI. Biochemical changes during development. *J. Biol. Chem.* 234:422–430.

19. Lee, B., M. Litt, and G. Buchsbaum. 1994. Rheology of the vitreous body: part 3. Concentration of electrolytes, collagen and hyaluronic acid. *Biorheology.* 31:339–351.

20. Denlinger, J. L., G. Eisner, and E. A. Balazs. 1980. Age-related changes in the vitreus and lens of rhesus monkeys (*Macaca mulatta*). *Exp. Eye Res.* 31:67–79.

21. Grimshaw, J., A. Kane, …, D. Archer. 1994. Quantitative analysis of hyaluronan in vitreous humor using capillary electrophoresis. *Electrophoresis.* 15:936–940.

22. Reardon, A., D. Heinegård, …, P. N. Bishop. 1998. The large chondroitin sulphate proteoglycan versican in mammalian vitreous. *Matrix Biol.* 17:325–333.

23. Lieleg, O., R. M. Baumgärtel, and A. R. Bausch. 2009. Selective filtering of particles by the extracellular matrix: an electrostatic bandpass. *Biophys. J.* 97:1569–1577.

24. Lieleg, O., I. Vladescu, and K. Ribbeck. 2010. Characterization of particle translocation through mucin hydrogels. *Biophys. J.* 98:1782–1789.

25. Lai, S. K., D. E. O'Hanlon, …, J. Hanes. 2007. Rapid transport of large polymeric nanoparticles in fresh undiluted human mucus. *Proc. Natl. Acad. Sci. USA.* 104:1482–1487.

26. Lai, S. K., Y. Y. Wang, …, J. Hanes. 2010. Nanoparticles reveal that human cervicovaginal mucus is riddled with pores larger than viruses. *Proc. Natl. Acad. Sci. USA.* 107:598–603.

27. Cu, Y., and W. M. Saltzman. 2009. Controlled surface modification with poly(ethylene)glycol enhances diffusion of PLGA nanoparticles in human cervical mucus. *Mol. Pharm.* 6:173–181.

28. Lieleg, O., and K. Ribbeck. 2011. Biological hydrogels as selective diffusion barriers. *Trends Cell Biol.* 21:543–551.

29. Peeters, L., N. N. Sanders, …, J. Demeester. 2005. Vitreous: a barrier to nonviral ocular gene therapy. *Invest. Ophthalmol. Vis. Sci.* 46:3553–3561.

30. Kim, H., S. B. Robinson, and K. G. Csaky. 2009. Investigating the movement of intravitreal human serum albumin nanoparticles in the vitreous and retina. *Pharm. Res.* 26:329–337.

31. Nance, E. A., G. F. Woodworth, …, J. Hanes. 2012. A dense poly(ethylene glycol) coating improves penetration of large polymeric nanoparticles within brain tissue. *Sci. Transl. Med.* 4:149ra119.

32. Schilling, J., E. Sackmann, and A. R. Bausch. 2004. Digital imaging processing for biophysical applications. *Rev. Sci. Instrum.* 75:2822–2827.

33. Dunderdale, G., S. Ebbens, …, J. Howse. 2012. Importance of particle tracking and calculating the mean-squared displacement in distinguishing nanopropulsion from other processes. *Langmuir.* 28:10997–11006.

34. Qian, H., M. P. Sheetz, and E. L. Elson. 1991. Single particle tracking. Analysis of diffusion and flow in two-dimensional systems. *Biophys. J.* 60:910–921.

35. Arends, F., R. Baumgärtel, and O. Lieleg. 2013. Ion-specific effects modulate the diffusive mobility of colloids in an extracellular matrix gel. *Langmuir.* 29:15965–15973.

36. Hiemenz, P. C., and R. Rajagopalan. 1997. Principles of Colloid and Surface Chemistry, 3rd ed. CRC Press, Boca Raton, FL.

37. Manning, G. S. 1969. Limiting laws and counterion condensation in polyelectrolyte solutions. I. Colligative properties. *J. Chem. Phys.* 51:924–933.

38. Rant, U., K. Arinaga, …, G. Abstreiter. 2003. Excessive counterion condensation on immobilized ssDNA in solutions of high ionic strength. *Biophys. J.* 85:3858–3864.

39. Pirie, A., G. Schmidt, and J. W. Waters. 1948. Ox vitreous humour. 1.—the residual protein. *Br. J. Ophthalmol.* 32:321–339.

40. Halfter, W., U. Winzen, …, A. Eller. 2006. Regulation of eye size by the retinal basement membrane and vitreous body. *Invest. Ophthalmol. Vis. Sci.* 47:3586–3594.

41. de Kozak, Y., K. Andrieux, …, P. Couvreur. 2004. Intraocular injection of tamoxifen-loaded nanoparticles: a new treatment of experimental autoimmune uveoretinitis. *Eur. J. Immunol.* 34:3702–3712.

42. Díaz-Llopis, M., M. J. Martos, …, F. J. Romero. 1992. Liposomally-entrapped ganciclovir for the treatment of cytomegalovirus retinitis in AIDS patients. Eperimental toxicity and pharmacokinetics, and clinical trial. *Doc. Ophthalmol.* 82:297–305.

43. Herrero-Vanrell, R., and M. F. Refojo. 2001. Biodegradable microspheres for vitreoretinal drug delivery. *Adv. Drug Deliv. Rev.* 52:5–16.

44. Peyman, G. A., B. Khoobehi, …, R. Fiscella. 1987. Intravitreal injection of liposome-encapsulated ganciclovir in a rabbit model. *Retina.* 7:227–229.

45. Shelke, N. B., R. Kadam, …, U. B. Kompella. 2011. Intravitreal poly(L-lactide) microparticles sustain retinal and choroidal delivery of TG-0054, a hydrophilic drug intended for neovascular diseases. *Drug Deliv. Transl. Res.* 1:76–90.

46. Bejjani, R. A., D. BenEzra, …, F. F. Behar-Cohen. 2005. Nanoparticles for gene delivery to retinal pigment epithelial cells. *Mol. Vis.* 11: 124–132.

47. Bourges, J. L., S. E. Gautier, …, F. F. Behar-Cohen. 2003. Ocular drug delivery targeting the retina and retinal pigment epithelium using polylactide nanoparticles. *Invest. Ophthalmol. Vis. Sci.* 44:3562–3569.

48. Radhika, M., K. Mithal, …, H. W. Flynn. 2014. Pharmacokinetics of intravitreal antibiotics in endophthalmitis. *J. Ophthalmic Inflamm. Infect.* 4:22.